Available online at www.sciencedirect.com
SCIENCE DIRECT®
International Journal of Heat and Mass Transfer 48 (2005) 5354–5370
International Journal of HEAT and MASS TRANSFER
www.elsevier.com/locate/ijhmt

Flame shapes and burning rates of spherical fuel particles in a mixed convective environment

V. Raghavan [1], V. Babu *, T. Sundararajan, R. Natarajan

Department of Mechanical Engineering, Indian Institute of Technology Madras, Chennai 600 036, India

Received 7 October 2004; received in revised form 6 July 2005
Available online 29 September 2005

Abstract

In this work, experimental and numerical investigations of spheres burning in a convective environment have been carried out. In the numerical simulations, transient axi-symmetric Navier–Stokes equations along with species and energy conservation equations are solved using a finite volume technique based on non-orthogonal semi-collocated grids. A global single step reaction involving two reactants, two products and one inert species together with an Arrhenius rate equation has been used to model kinetics. For the sake of comparison, an infinite rate chemistry model has also been attempted. The density of the mixture has been evaluated from ideal gas equation of state. Thermo-physical properties like thermal conductivity and viscosity have been evaluated using the Chapman–Enskog description of binary gas mixtures. Specific heats and species enthalpies have been evaluated using piece-wise polynomials of temperature. The burning of isolated spherical particles in a mixed convective environment at atmospheric pressure has been simulated for various particle sizes, free-stream velocities and ambient temperatures. The numerical predictions have been compared with experimental results obtained using the porous sphere technique and the agreement is found to be good. Correlations have been developed for the critical Reynolds number at which transition from the envelope to wake flame occurs and also for the mass burning rates at sub-critical or super-critical Reynolds number regimes. It is observed that, at higher ambient temperatures, transition to wake flame is delayed to a higher critical Reynolds number value. The infinite rate chemistry model predicts flame shapes and mass burning rates with reasonable accuracy in the sub-critical Reynolds number regime, but it fails to predict transition to wake flame shape. For analyzing transition phenomena, a finite rate chemistry model is required.

1. Introduction

Diffusion combustion of spherical particles occurs in several practical combustors. Pulverized coal particles are burnt in an oxidizing gas medium in the boilers of power plants and in metallurgical furnaces. A spray of fuel droplets is fired in oil-fired furnaces and in gas turbine combustors. Quasi-steady combustion models for the burning of stationary particles have been developed in the past, for pulverized solid fuel particles [1–3] and for isolated liquid fuel droplets [4–6], in which the transport processes inside the particles are neglected. These quasi-steady models are applicable for the low pressure burning of fuel particles, after the initial ignition and internal heating transients are over. Verification for the

* Corresponding author. Tel.: +91 44 22574688.
E-mail address: vbabu@iitm.ac.in (V. Babu).
[1] Present address: University of Nebraska-Lincoln, Lincoln, USA.

0017-9310/$ - see front matter © 2005 Elsevier Ltd. All rights reserved.
doi:10.1016/j.ijheatmasstransfer.2005.07.029

Nomenclature

D	mass diffusivity in (m^2/s)
Fr	Froude number ($u_\infty/\sqrt{gd}$)
g	acceleration due to gravity (m/s^2)
h	total enthalpy (kJ/kg)
k	thermal conductivity (W/mK)
l	length of a control volume cell (m)
n	normal vector
p	pressure (N/m^2)
Pr	Prandtl number (υ/α)
Ri	Richardson number ($g\beta\Delta Td/u_\infty^2$)
Re	Reynolds number ($\rho u_\infty d/\mu$)
Sc	Schmidt number (υ/D)
T	temperature (K)
u, v	axial and radial velocity components (m/s)
V_{cell}	volume of the cell (m^3)
X	mole fraction
x, r	axial and radial coordinates (m)
Y	mass fraction
Δt	time step (s)

Greek symbols

α	thermal diffusivity (m^2/s)
ρ	density (kg/m^3)
μ	coefficient of viscosity ($N\,s/m^2$)
σ, τ	normal and shear stresses (N/m^2)
$\tau_{reaction}$	reaction time scale (s)
ϕ	mixture fraction
$\dot{\omega}$	mass based reaction rate ($kg/m^3\,s$)

Subscripts

i	species i
m	gas mixture
s	droplet surface
∞	free-stream conditions
ref	reference quantities; properties evaluated at free-stream conditions

quasi-steady burning of isolated, spherical fuel particles has been carried out using the porous sphere technique [7,8]. The effect of a convective flow field on the rate of burning of liquid droplets has been investigated by several authors in the past [9,10]. Recently, Balakrishnan et al. [11,12] investigated the quasi-steady burning of spherical particles in a mixed convective environment, at low Reynolds numbers. The existence of an envelope diffusion flame was assumed in these studies. Burning of a coal particle in low Reynolds number regime has been studied by Blake [13]. Here, the effect of viscous flow over a spherical carbon particle has been presented. Transient evaporation studies for fuel droplets in normal as well as microgravity environment under low or high ambient pressure and high ambient temperature conditions have been carried out by several authors [14–18]. These authors have considered variable thermo-physical properties, liquid phase species conservation, and the effect of pressure on droplet vaporization. The burning of fuel droplets in a high temperature turbulent jet flow environment has been considered by Szekely and Faeth [19]. This study correlates the local drop gasification rate as a function of mixture fraction in a turbulent environment similar to the condition within combusting sprays.

In practical combustors, the Reynolds number based on particle size and relative velocity between the surrounding medium and the particle could be in the range of 1000. At this Reynolds number, an envelope flame does not exist around the particle and the reaction zone corresponds to that of a wake flame. For still higher Reynolds numbers, even the wake flame may be blown-off. Detailed theoretical modeling of such transitions during the diffusion combustion of fuel particles is not available at present.

In the present study, a model is described for the transient simulation of a fuel particle burning in convective atmosphere. The salient features of the model are: use of non-orthogonal control volumes with semi-collocated mesh, generalized interpolation of all flow and transport variables in a cell, finite rate chemistry and detailed evaluation of thermo-physical properties based on local temperature and species concentrations. Numerical results have been obtained for a range of mixed convective flow conditions and some of the predictions have been validated with results obtained from the porous sphere experiment.

2. Problem formulation

In order to simplify the otherwise complex problem of modeling combustion of a fuel particle, the following assumptions have been made:

1. Flow is axi-symmetric and laminar.
2. Ideal-gas mixture formulation is used to account for density variations with temperature and concentration. However, the incompressible flow solution methodology has been adopted to derive the pressure field, as velocity values are very small.
3. Only the gas phase region has been modeled in a decoupled manner, assuming no slip boundary condition and no particle heating effects at the particle surface. These approximations are applicable to the low

pressure burning of a fuel particle, during the quasi-steady burning period.
4. Single component fuel undergoing complete combustion through a global reaction step has been considered. Only gas-phase combustion is studied, assuming high fuel volatility.
5. Chapman–Enskog description for binary gas mixtures has been used to evaluate thermo-physical properties such as thermal conductivity and viscosity. Piece-wise polynomials in temperature have been used to evaluate specific heats and species enthalpies.
6. Thermal radiation effects are neglected, which amounts to assuming a non-luminous flame.
7. The partial pressure of vapor adjacent to the particle surface is assumed to be equal to the vapor pressure of the fuel at the interface temperature.

A theoretical analysis incorporating the above assumptions can be employed primarily for modeling the burning of isolated liquid fuel particles, and for the combustion of solid fuel particles to a limited extent (when combustion occurs in gas phase).

The governing equations are non-dimensionalized using appropriate length, velocity and time scales. The free-stream velocity (u_∞) is chosen as reference velocity. The particle diameter d is used as reference length scale and the ratio of particle diameter to free-stream velocity is used as the time scale. All the other variables have been made dimensionless by combining these three reference quantities with the appropriate free-stream parameters. The dimensionless variables are listed below:

Coordinates:

$$x = \frac{x^*}{d}, \quad r = \frac{r^*}{d}, \quad t = \frac{t^* u_\infty}{d}$$

Flow variables:

$$u = \frac{u^*}{u_\infty}, \quad v = \frac{v^*}{u_\infty}, \quad \rho = \frac{\rho^*}{\rho_\infty}, \quad p = \frac{p^*}{\rho_\infty u_\infty^2},$$
$$T = \frac{T^* - T_\infty}{T_\infty}, \quad h = \frac{h^*}{C_{P_{\mathrm{ref}}} T_\infty}$$

Transport variables and physical properties:

$$\mu = \frac{\mu^*}{\mu_{\mathrm{ref}}} \frac{\mu_{\mathrm{ref}}}{\rho_\infty u_\infty d} = \frac{\mu^*}{\mu_{\mathrm{ref}}} \frac{1}{Re_\infty}, \quad C_P = \frac{C_P^*}{C_{P_{\mathrm{ref}}}},$$
$$D_{\mathrm{im}} = \frac{D_{\mathrm{im}}^*}{D_{\mathrm{ref}}} \frac{D_{\mathrm{ref}} \nu_{\mathrm{ref}}}{\nu_{\mathrm{ref}} u_\infty d} = \frac{D_{\mathrm{im}}^*}{D_{\mathrm{ref}}} \frac{1}{Re_\infty Sc_\infty},$$
$$k = \frac{k^*}{k_{\mathrm{ref}}} \frac{k_{\mathrm{ref}}}{\rho_\infty u_\infty C_{P_{\mathrm{ref}}} d} = \frac{k^*}{k_{\mathrm{ref}}} \frac{1}{Re_\infty Pr_\infty}$$

Rate of reaction:

$$\dot{\omega}_i = \frac{\dot{\omega}_i^* d}{\rho_\infty u_\infty}$$

Variables with the superscript $*$ in the above equations denote dimensional quantities.

2.1. Governing equations

The dimensionless governing equations for mass, momentum, species and energy conservation in the gas phase are given below in flux form for each control volume cell, in cylindrical polar coordinates. For quasi-steady burning regime, the effects of transport processes within the particle are negligible [11].

2.1.1. x-momentum equation

$$\frac{\mathrm{d}}{\mathrm{d}t}(\rho u) V_{\mathrm{cell}} + \oint \rho u (u n_x + v n_r) 2\pi r \, \mathrm{d}l = \oint (\sigma_{xx} n_x + \tau_{rx} n_r) 2\pi r \, \mathrm{d}l + \frac{1}{Fr^2}\left(1 - \frac{\rho}{\rho_\infty}\right) V_{\mathrm{cell}} \quad (1)$$

where, V_{cell} is the volume of the cell and Fr is the Froude number. It should be noted here that the x-axis points vertically upwards (see, Fig. 1) and the last term in the above equation arises from buoyancy effects. In the case of a downward forced convective flow (in negative x-direction), the buoyancy force will be of opposite sense. For large-sized particles (few mm diameter), free convective effects could also be important, in addition to forced convection.

2.1.2. r-momentum equation

$$\frac{\mathrm{d}}{\mathrm{d}t}(\rho v) V_{\mathrm{cell}} + \oint \rho v (u n_x + v n_r) 2\pi r \, \mathrm{d}l = \oint (\tau_{rx} n_x + \sigma_{rr} n_r) 2\pi r \, \mathrm{d}l - \frac{\sigma_{\theta\theta}}{r} V_{\mathrm{cell}} \quad (2)$$

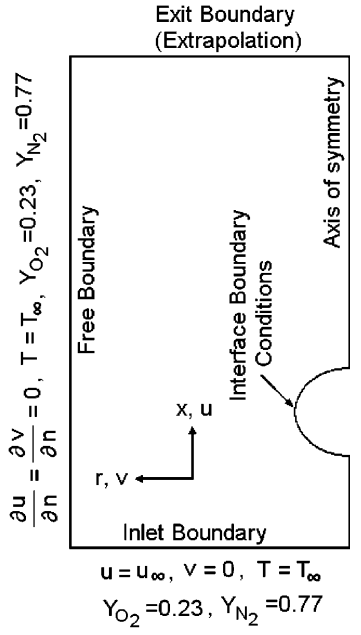

Fig. 1. Computational domain.

The stress terms in the above equations can be written as

$$\sigma_{xx} = -p + 2\frac{\mu}{\mu_{\text{ref}}}\frac{1}{Re_\infty}\frac{\partial u}{\partial x},$$

$$\sigma_{rr} = -p + 2\frac{\mu}{\mu_{\text{ref}}}\frac{1}{Re_\infty}\frac{\partial v}{\partial r},$$

$$\sigma_{\theta\theta} = -p + 2\frac{\mu}{\mu_{\text{ref}}}\frac{1}{Re_\infty}\frac{v}{r},$$

$$\tau_{rx} = \tau_{xr} = \frac{\mu}{\mu_{\text{ref}}}\frac{1}{Re_\infty}\left(\frac{\partial u}{\partial r} + \frac{\partial v}{\partial x}\right)$$

2.1.3. Species conservation equation

Here, both infinite rate chemistry and finite rate chemistry models have been used. In the former, the reaction is assumed to be infinitely fast and the reaction zone is very thin. In the latter, an Arrhenius type of equation for single step reaction between the fuel vapor and oxygen has been employed.

2.1.3.1. Infinite rate chemistry model. For a global single step reaction given by

1 kg of Fuel + s kg of Oxidizer

$\rightarrow (1 + s)$ kg of Products,

the mixture fraction (ϕ) can be defined as

$$\phi = \frac{(sY_{\text{F}} - Y_{\text{ox}}) - (sY_{\text{F}} - Y_{\text{ox}})_0}{(sY_{\text{F}} - Y_{\text{ox}})_1 - (sY_{\text{F}} - Y_{\text{ox}})_0} \tag{3}$$

where subscript 0 denotes oxidizer stream and 1 denotes fuel stream. The conservation equation for the mixture fraction is written as

$$\frac{\mathrm{d}}{\mathrm{d}t}(\rho\phi)V_{\text{cell}} + \oint \rho\phi(un_x + vn_r)2\pi r\,\mathrm{d}l = \rho\frac{D}{D_{\text{ref}}}\frac{1}{Re_\infty Sc_\infty}\left(\oint\left(\frac{\partial\phi}{\partial r}n_r + \frac{\partial\phi}{\partial x}n_x\right)2\pi r\,\mathrm{d}l\right) \tag{4}$$

2.1.3.2. Finite rate chemistry model. Here a global single step reaction with 5 species (Fuel, oxygen, CO_2, H_2O, N_2) has been considered. For a particular species "i", the species conservation equation is of the form,

$$\frac{\mathrm{d}}{\mathrm{d}t}(\rho Y_i)V_{\text{cell}} + \oint \rho Y_i(un_x + vn_r)2\pi r\,\mathrm{d}l = \oint \rho\frac{D_{\text{im}}}{D_{\text{ref}}}\frac{1}{Re_\infty Sc_\infty}\left(\frac{\partial Y_i}{\partial x}n_x + \frac{\partial Y_i}{\partial r}n_r\right)2\pi r\,\mathrm{d}l + \dot{\omega}_i V_{\text{cell}} \tag{5}$$

with $\dot{\omega}_i^*$ denoting the mass rate of production of species i per unit volume.

2.1.4. Energy conservation equation

The energy conservation equation in flux form is given by,

$$\frac{\mathrm{d}}{\mathrm{d}t}(\rho C_P T)V_{\text{cell}} + \oint \rho C_P T(un_x + vn_r)2\pi r\,\mathrm{d}l = \frac{1}{Re_\infty Pr_\infty}\left(\oint\frac{k}{k_{\text{ref}}}\left(\frac{\partial T}{\partial r}n_r + \frac{\partial T}{\partial x}n_x\right)2\pi r\,\mathrm{d}l\right) - \sum_{i=1}^{n}\dot{\omega}_i h_{fi}V_{\text{cell}} + \left(\sum_{i=1}^{n}\oint\rho\frac{D_{\text{im}}}{D_{\text{ref}}}\frac{1}{Re_\infty Sc_\infty}C_{Pi}T \times \left(\frac{\partial Y_i}{\partial r}n_r + \frac{\partial Y_i}{\partial x}n_x\right)2\pi r\,\mathrm{d}l\right) \tag{6}$$

In the above equation h_{fi} is the enthalpy of formation for ith species.

2.2. Boundary conditions

With reference to Fig. 1, the following conditions have been specified at the boundaries:

(1) *Inlet*: Atmospheric air with uniform velocity u_∞ and temperature T_∞ enters the domain. The mass fractions of oxygen and nitrogen correspond to those of normal air. Hence at inlet, $u = u_\infty$, $v = 0$, $Y_{\text{ox}} = 0.23$, $Y_{\text{fuel}} = 0$, $Y_{N_2} = 0.77$, and $T = T_\infty$.

(2) *Axis of symmetry*: $\dfrac{\partial u}{\partial r} = 0$, $v = 0$, $\dfrac{\partial T}{\partial r} = 0$, $\dfrac{\partial Y_i}{\partial r} = 0$, $\dfrac{\partial \phi}{\partial r} = 0$.

(3) *Far stream and exit*: Due to combustion reactions occurring in the vicinity of the sphere, the outgoing fluxes of species (at the outlet boundary) will not be equal to the net incoming fluxes into the computational domain. Therefore, the selection of an appropriate exit boundary condition is non-trivial. In the present work, all the solution variables have been extrapolated in the direction normal to the boundary using three point polynomial fits. In addition, the extrapolated solution thus obtained on the boundary has also been locally smoothened by considering all the neighbors of the node. After considerable numerical experimentation, the inlet, far stream and exit boundaries have been located at 4, 6 and 16 diameters respectively from the particle centre.

(4) *Particle surface*:

(a) Assuming thermodynamic equilibrium at the interface, the partial pressure of fuel vapor can be equated to the vapor pressure at the interface temperature. In turn, the mole fraction of fuel adjacent to the particle surface can be written as

$$X_{\text{Fs}} = \frac{P_{\text{sat}}}{P_{\text{atm}}} = \exp\left[-\frac{h_{\text{fg}}\text{MW}_{\text{fuel}}}{R_{\text{u}}}\left(\frac{1}{T} - \frac{1}{T_b}\right)\right]$$

using the Clausius–Clayperon equation. The mass fraction of fuel is given as

$$Y_{\text{Fs}} = X_{\text{Fs}}\frac{\text{MW}_{\text{fuel}}}{\text{MW}_{\text{mixture}}}$$

where MW denotes the molecular weight.

(b) The total fuel mass flow rate at the surface is equal to the sum of the fuel mass flow rates due to convection and diffusion. The local evaporation velocity v_s can, therefore, be evaluated as

$$\rho_s v_s = \rho_s v_s Y_{Fs} + \left(-\rho_s D_s \left(\frac{\partial Y_F}{\partial r}\right)_s\right) \Rightarrow v_s = \frac{-D_s \left(\frac{\partial Y_F}{\partial r}\right)_s}{1 - Y_{Fs}}$$

(c) Assuming no internal heating (after the attainment of quasi-steady burning) heat balance at the interface can be written as

$$k\frac{dT}{dr} = \rho v_s h_{fg}$$

2.3. Evaluation of thermo-physical properties with temperature

Mass density (ρ), viscosity (μ), thermal conductivity (k) and binary mass diffusivity (D_{AB}) are evaluated as follows:

$$\rho = \frac{p}{R_u T} MW_{mix} \tag{7a}$$

where R_u is the universal gas constant and MW_{mix} is the molecular weight of the mixture. The transport properties of each species can be calculated as

$$\mu = \frac{2.6693 \times 10^{-6}\sqrt{T \times MW}}{\sigma^2 \Omega_\mu} \tag{7b}$$

The thermal conductivity (k) and binary diffusivity (D_{AB}) are given as

$$k = \left(C_P + \frac{5}{4}\frac{R_u}{MW}\right) \times \mu \tag{7c}$$

$$D_{AB} = \frac{0.0266\sqrt{T^3}}{P\sqrt{MW_{AB}}\sigma_{AB}^2 \Omega_D}, \quad \text{where } \sigma_{AB} = \frac{\sigma_A + \sigma_B}{2}\ \text{Å}. \tag{7d}$$

In the above expressions the Lennard-Jones parameters σ_{AB} and Ω_D have been taken from the literature [21].

In order to evaluate the specific heat of each species, piece-wise polynomials in temperature have been employed as given below:

$$C_P = aT + bT^2 + cT^3 + dT^4$$

The mixture properties are evaluated [21] as follows:

$$C_P = \sum_i C_{Pi} Y_i \tag{8}$$

$$\mu_{mix} = \sum_{i=1}^{n} \frac{Y_i \mu_i}{\sum_{j=1}^{n} Y_j \phi_{ij}} \quad \text{and} \quad k_{mix} = \sum_{i=1}^{n} \frac{Y_i k_i}{\sum_{j=1}^{n} Y_j \phi_{ij}} \tag{9}$$

where Y is the mass fraction and

$$\phi_{ij} = \frac{1}{\sqrt{8}}\left(1 + \frac{MW_i}{MW_j}\right)^{-\frac{1}{2}}\left[1 + \sqrt{\frac{\mu_i}{\mu_j}}\left(\frac{MW_j}{MW_i}\right)^{\frac{1}{4}}\right]^2$$

2.4. Finite rate chemistry model—evaluation of reaction rate

Here, a single step global reaction, with two reactants (fuel and oxygen), two products (Carbon-dioxide and water vapor) and one inert species (nitrogen) is considered. In both the numerical and experimental investigations of the present study, methanol has been used as the fuel. A single step chemical reaction is taken in the form

$$CH_3OH + 1.5(O_2 + 3.76N_2) \xrightarrow{K} CO_2 + 2H_2O + 5.64N_2$$

The rate constant K is evaluated from the Arrhenius relation

$$K = AT^m \exp\left(\frac{-E_a}{R_u T}\right)$$

where A is the pre-exponential factor and E_a is the activation energy. The rate of the reaction is given by

$$\dot{\omega} = K[CH_3OH]^{n_1}[O_2]^{n_2}\frac{\text{kmol}}{\text{m}^3\,\text{s}} \tag{10}$$

The values of A, E_a, m, n_1 and n_2 have been obtained from Turns [22] for the above reaction ($A = 1.799 \times 10^{10}$, $E_a = 1.256 \times 10^8$, $n_1 = 1.25$, $n_2 = 0.5$ and $m = 0$). After evaluating the rate of the reaction, the mass rate of production or destruction for any species can evaluated as follows:

$$\dot{\omega}_i = (\pm \upsilon_i)\dot{\omega} MW_i$$

where υ_i is the stoichiometric coefficient of the ith species in the single step global reaction. The positive or negative sign in the rate expression is chosen depending on whether the species is a reactant or a product. For any given fuel, a procedure similar to above can be adopted, with appropriate values of the kinetic parameters for the single step global reaction model.

3. Solution procedure

The governing equations have been discretized using the Finite Volume Method. A non-orthogonal grid with semi-collocated, four noded quadrilateral cells (Fig. 2) has been employed for the numerical calculations. Within each non-orthogonal cell, the variables are interpolated with general bilinear interpolation functions, used commonly in Finite Element Method [11]. A brief description of the solution procedure is given here. Details of the evaluation of fluxes and derivatives and discretization of the integral form of governing equations are available elsewhere [20].

The velocity components are obtained by integrating the momentum equations, using an explicit time marching scheme with an assumed pressure field $\tilde{p}$. These

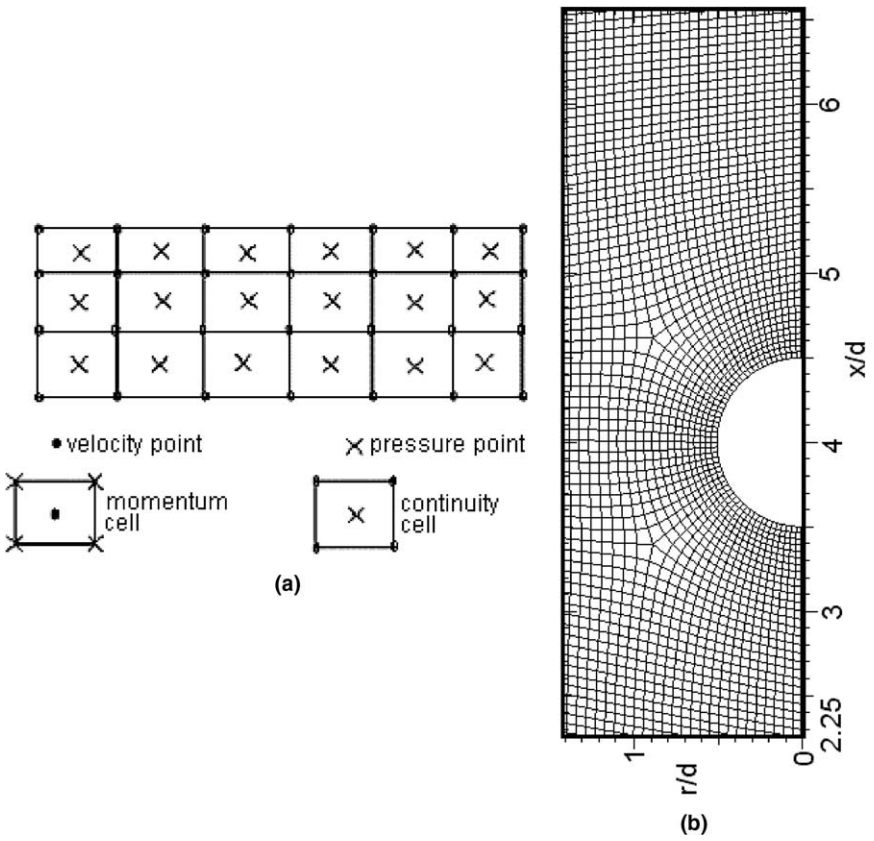

Fig. 2. (a) Semi-collocated grid and (b) discretized domain (close up view).

velocities will usually not satisfy the continuity equation. Hence, the mass residue for each continuity cell is evaluated and the associated pressure corrections are obtained by solving the pressure Poisson equation of the form

$$\nabla^2 p' = \frac{\rho}{\Delta t}\left(\frac{\partial u}{\partial x} + \frac{1}{r}\frac{\partial}{\partial r}(rv)\right)$$

where, the right hand side term represents the continuity equation residue. After integrating the pressure correction equation over the continuity cells, the resulting pressure gradient terms across the cell boundaries are evaluated using the general interpolation schemes, to yield a set of simultaneous algebraic equations in terms of p'. The cell pressures are then updated as $p^{n+1} = \tilde{p} + p'$ and the velocities are also updated by solving the momentum equations again with the updated pressure field.

Mass/mixture fraction equations along with the energy equation are solved using the explicit time marching scheme with a smaller time step value for a certain number of inner iterations. The thermo-physical properties are updated using Eqs. (7)–(9). The chemical kinetic equation (10) is solved to obtain the reaction rate at the updated temperature. This transient marching procedure is carried out until either the steady state or a time independent oscillatory solution is obtained. For the finite rate chemistry model, initially, a certain number of iterations are carried out (for flow solution alone) without solving the energy and reaction rate equations. After obtaining the cold flow solution, a suitable high temperature region is then patched near the particle, so that ignition can occur followed by combustion. Then, by time marching, the complete set of equations is solved.

The solution methodology outlined above has been implemented using a FORTRAN code and computations have been carried out on Intel Pentium III processor based Personal computers, SGI workstations and HP cluster machines. A grid sensitivity study with 16 000, 22 000 and 32 000 cells has shown that a grid with 22 000 cells gives a good balance between computational economy and solution accuracy. For most of the cases, the time step size is 1.0e−05 seconds and it takes about 30 000 time steps to have either a converged solution or obtain enough cycles in the unsteady solution. Each computation required about 10 h of wall clock time on the Pentium based PCs.

4. Experimental procedure

Experimental investigation of spherical particle combustion has been carried out using the porous sphere technique. The experimental setup consisting of the liquid fuel feed system, wind tunnel and porous sphere is shown in Fig. 3.

Porous alundum spheres are prepared from four parts by volume of white aluminium oxide (Chromatographic grade) of grain size 10–15 μm, one part by volume of powdered fire clay, two drops of silica gel and a small amount of water. The porosity of the sphere can be increased, if necessary, by increasing the fire clay content suitably. The spheres are dried in air and then cured in a furnace at 1000 K for about 5 h. After cooling, a small hole is drilled carefully for inserting the free end of the supporting tube. A stainless steel hypodermic needle of diameter 1.2 mm has been used to support the alundum sphere. Uniform distribution of fuel inside the porous sphere is ensured by drilling radial holes of 0.4 mm diameter at the end of the hypodermic needle. The other end of the needle is fixed to a glass syringe. An infusion pump is used to supply the fuel, which pushes the glass syringe at the desired speed. The volume flow rate from the syringe is directly shown by the digital display of the infusion pump. The sphere is supported in front of an air flow system, which consists of a low turbulence wind tunnel of 200 mm diameter. The supply air line is fitted with an orifice plate to measure the flow rate. The velocity of the air flow at the tunnel exit has been calibrated in terms of the pressure drop across the orifice, using a pitot tube connected to a digital manometer. Mass burning rate is measured by noting down the fuel flow rate (ml/h) from the syringe when the following conditions are satisfied: The fuel should not drip from the burning sphere and still the entire surface of the particle should be wet. A steady flame should prevail during the combustion process. The fuel mass flow rate can be measured within an error of ±2% with the help of the infusion pump. Photographs of the flames at different free-stream velocities have been taken and processed in an image-processor to get the flame shape assuming that it corresponds to the surface of maximum luminosity.

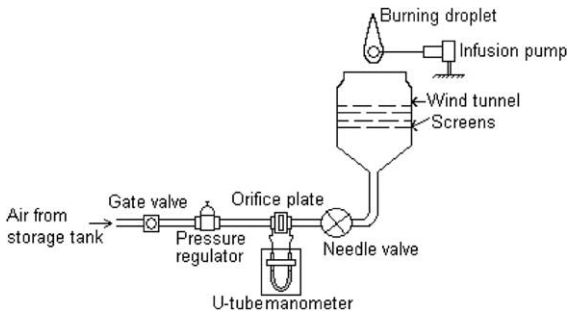

Fig. 3. Porous sphere experimental setup.

5. Results and discussion

In this section, mass burning rates and flame shapes are presented for different values of particle size, free-stream air velocity, and ambient temperature.

5.1. Validation

Case 1: Results from experiments and numerical simulations for a single fuel particle of 8 mm diameter burning in a free-stream with velocity 0.4, 0.6 or 0.8 m/s at room temperature are presented in Figs. 4 and 5. Flame shapes obtained by the infinite rate and finite rate chemistry models are compared with the experimentally observed flame shape in Fig. 4 for a free-stream velocity of 0.4 m/s. It is evident that both infinite and finite rate chemistry models give accurate results for this diffusion dominated envelope flame. The contour of the mixture fraction corresponding to stoichiometric value is designated as the flame surface in the infinite rate chemistry model. In the finite rate chemistry model, due to small leakage across the flame, the region corresponding to the oxygen mass fraction range of 0.02–0.002 is identified as the flame zone and the locus of the mid point of this zone is designated as the flame surface. The mass burning rate predictions from the two models also agree

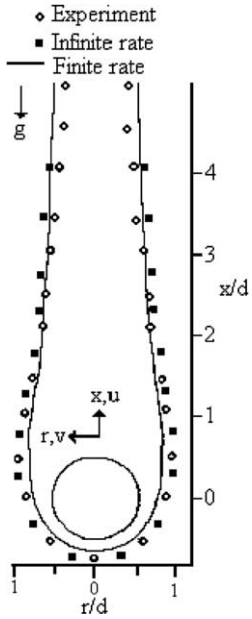

Fig. 4. Validation of flame shapes ($Re = 200$, $T_\infty = 300$ K, $d = 8$ mm, $u_\infty = 0.4$ m/s).

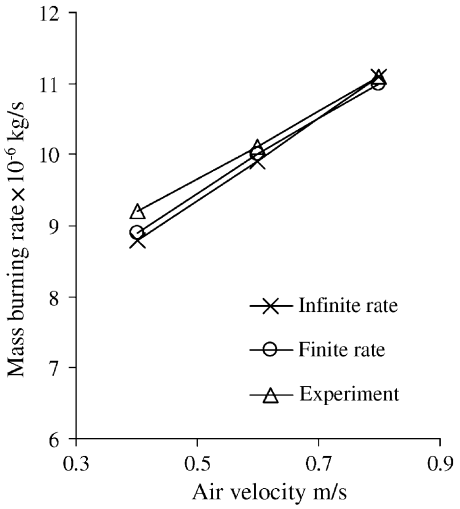

Fig. 5. Validation of mass burning rates ($T_\infty = 300$ K).

well with the corresponding experimental data shown in Fig. 5 at different free-stream velocities.

Case 2: Flame shapes obtained from numerical simulations using infinite rate chemistry model for the case of an 8 mm diameter particle at free-stream velocities of 0.4 m/s and 0.8 m/s in the negative x-axis direction (downward flow) are shown in Fig. 6. Experimental results of Balakrishnan et al. [12] are also shown in this figure for comparison. In this case of envelope flame also, the comparison between the numerical results and the experimental data is quite good. In fact, for the higher free-stream velocity value of 0.8 m/s, a flattened cylindrical flame shape is obtained, due to the opposing effects of buoyancy and forced convection phenomena (Fig. 6(b)).

Case 3: At higher values of free-stream air velocities, envelope flame does not occur, as there is no combustion in the front portion of the sphere. Instead, the flame stabilizes in the wake region. This can be seen in Figs. 7(a) and (b) and 8(A), for a particle diameter of 12.2 mm burning under different free-stream velocities. These calculations have been performed using the finite rate chemistry model since the infinite rate chemistry model could not simulate wake flames. Thus, it is evident that extinction of the flame in the front portion of the sphere occurs, because the flow residence time is less than the reaction time; in the wake region where flow separation results in recirculation, flame is stabilized because of larger residence time for reactants. To illustrate this and to correlate the effect of flow field on flame shape, a comparison of stream lines and flame shapes around an 8 mm diameter particle under different free-stream velocities have been shown in Fig. 9. It is clearly seen that after transition from envelope to wake flame, the flame stabilizes in the recirculation zone at the rear

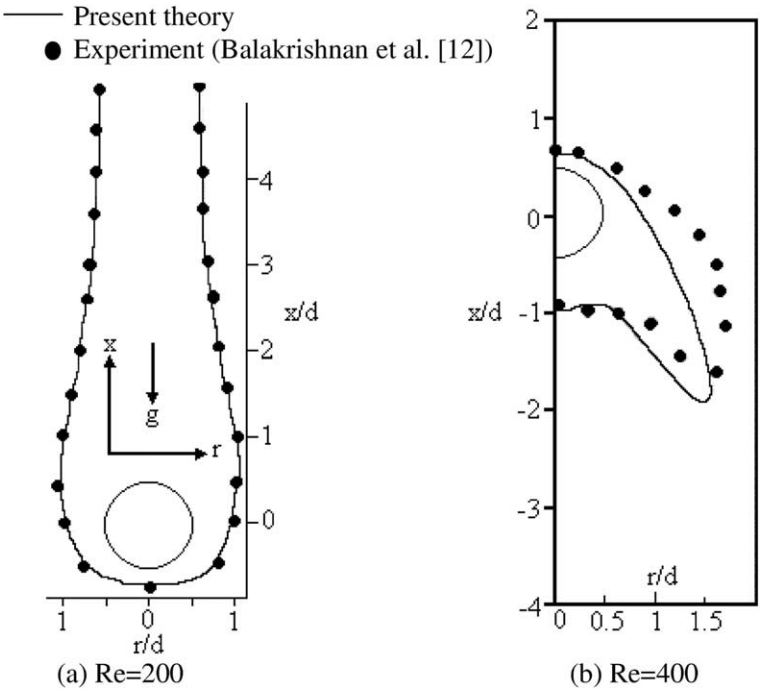

Fig. 6. Flame shapes for free-stream velocity of (a) 0.4 m/s and (b) 0.8 m/s in the negative x-direction and $T_\infty = 300$ K, using infinite rate chemistry model.

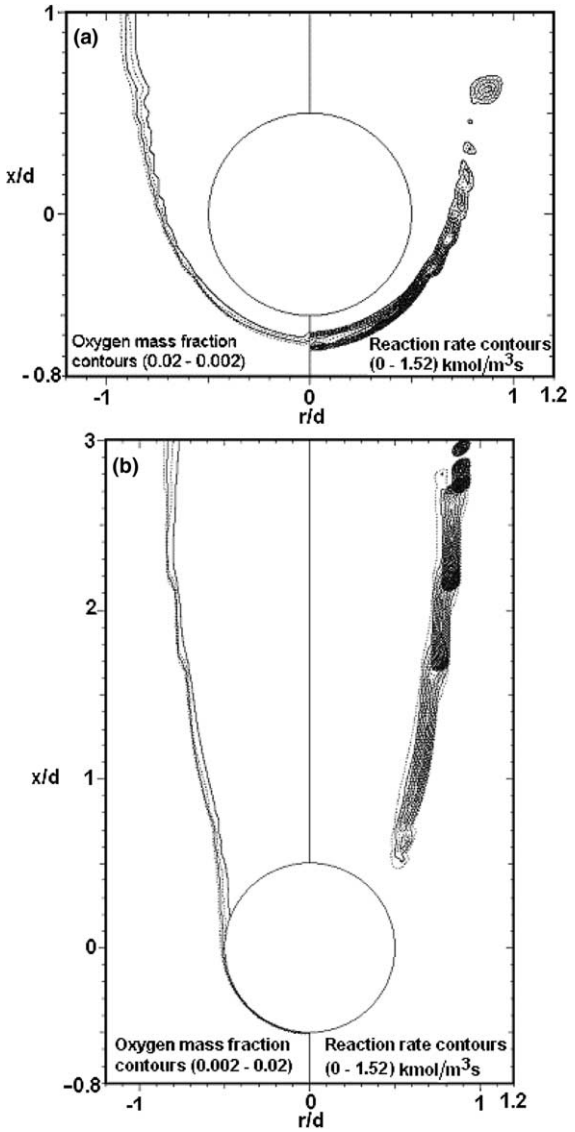

Fig. 7. (a) Contours of oxygen mass fraction and reaction rates for a case with $Re = 1960$ (particle diameter of 12.2 mm and free-stream air velocity 1.2 m/s), representing envelope flame. (b) Contours of oxygen mass fraction and reaction rates for a case with $Re = 6530$ (particle diameter of 12.2 mm and free-stream air velocity 4 m/s), representing wake flame.

portion of the spherical particle. Oxygen mass fraction contours with values in the range 0.002–0.02 have been used to delineate the flame zone in Figs. 7 and 8. Comparisons of oxygen mass fraction contours with values in the above-mentioned range and the contours of reaction rate, have been shown in Fig. 7(a) and (b), for the burning of a 12.2 mm particle with free-stream velocities 1.2 m/s and 4 m/s. The figures clearly show that the reaction zone (i.e. flame region) is captured well by contours of oxygen mass fraction in the range of 0.002–0.02.

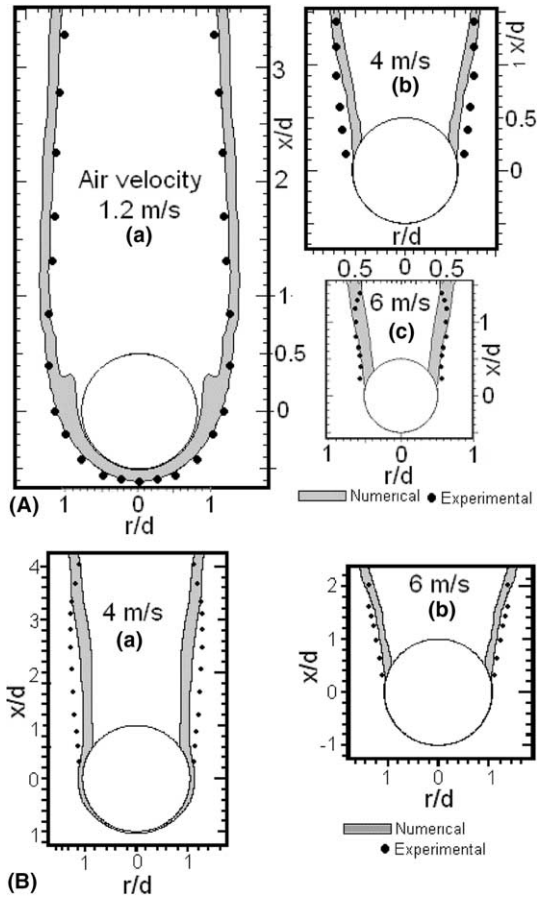

Fig. 8. (A) Validation of flame shapes for a particle diameter of 12.2 mm, with Reynolds numbers (a) 1960, (b) 6530 and (c) 9796, using finite rate chemistry model. (B) Validation of flame shapes for a particle diameter of 16.4 mm, with Reynolds numbers (a) 8800 and (b) 13200, using finite rate chemistry model.

The Reynolds numbers corresponding to the free-stream velocity of 1.2 m/s, 4 m/s and 6 m/s are 1960, 6530 and 9796 respectively, based on free-stream properties. It is evident here that the transition from envelope flame to wake flame occurs between $Re = 1960$ and $Re = 6530$, for the cases studied here. Similar trends are seen for a particle diameter of 16.4 mm in Fig. 8(B) corresponding to the free- stream Reynolds number values of 8800 ($u_\infty = 4$ m/s) and 13200 ($u_\infty = 6$ m/s).

Although one would expect transition towards turbulent flow at such high Reynolds numbers, the good agreement seen for the flame shapes obtained using a laminar code, can be attributed to the local Reynolds number (close to the particle) being much less than Re_∞. The minor deviations observed between the experimental (Fig. 10) and numerically simulated flame shapes could be due to the flow-interference caused by the support for the sphere.

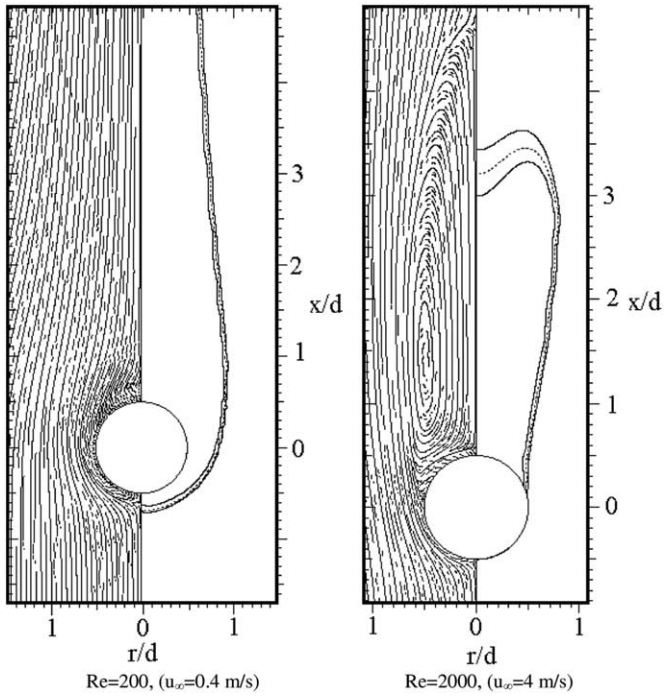

Fig. 9. Comparison of flow-field and flame shapes for a particle diameter of 8 mm, using finite rate chemistry model for different Reynolds numbers.

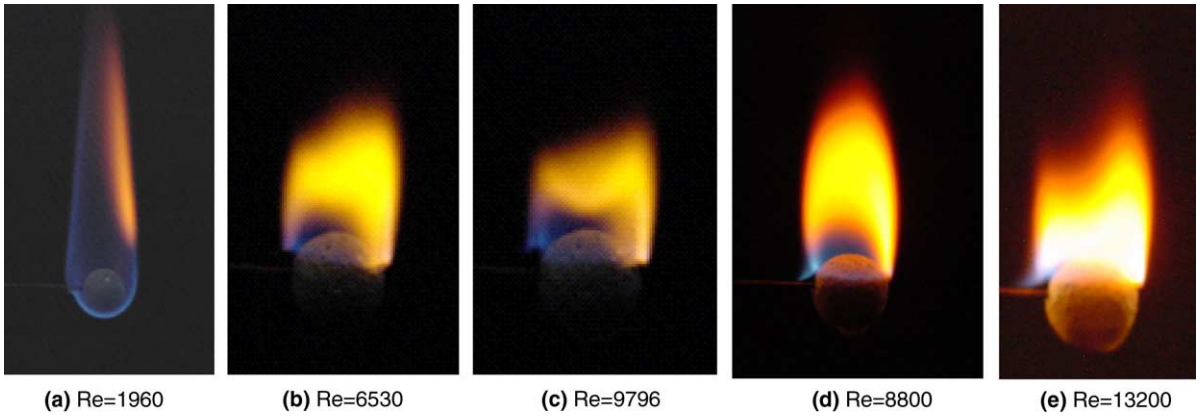

Fig. 10. Flame photographs for particle diameters of (a–c) 12.2 mm, (d,e) 16.4 mm, and free-stream velocities of (a) 1.2 m/s, (b,d) 4.0 m/s and (c,e) 6.0 m/s.

Photographs of flame shapes observed during the experiments corresponding to the cases in Fig. 8 are shown in Fig. 10. The flame shapes predicted by the numerical calculations agree very well with those seen in the experiments.

5.2. Effects of free-stream velocity

5.2.1. Variation of mass burning rate

The variations of mass burning rate with free-stream air velocity for spherical particles of diameter 8 mm and 10.8 mm are shown in Fig. 11. As the free-stream velocity increases, the mass burning rate increases in general; however, near the critical value at which the transition from envelope flame to wake flame occurs, there is a sudden reduction in the mass burning rate as seen in Fig. 11, due to reduction in the flame surface area. After transition, the mass burning rate again increases with free-stream velocity. This trend is observed for the larger sphere also, but at higher values of mass burning rates. These results are consistent with the results reported in [19], where it

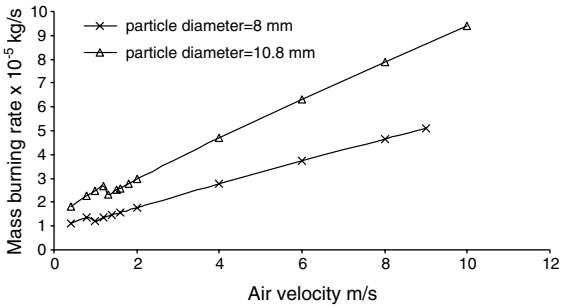

Fig. 11. Variation of mass burning rate with free-stream air velocity.

is stated that the evaporation rate increases with particle diameter.

5.2.2. Variation of flame shape

The flame shapes for a 10.8 mm sphere burning in different free-stream velocity conditions (ranging from 0.4 m/s to 8 m/s) are shown in Fig. 12. The Reynolds number varies in the range 288–5760. The contour line corresponding to the oxygen mass fraction of 0.011 has been used to delineate the flame surface in these figures. At low free-stream velocities, the flame envelopes the particle. The flame standoff distance in the front part of the sphere decreases as the free-stream velocity

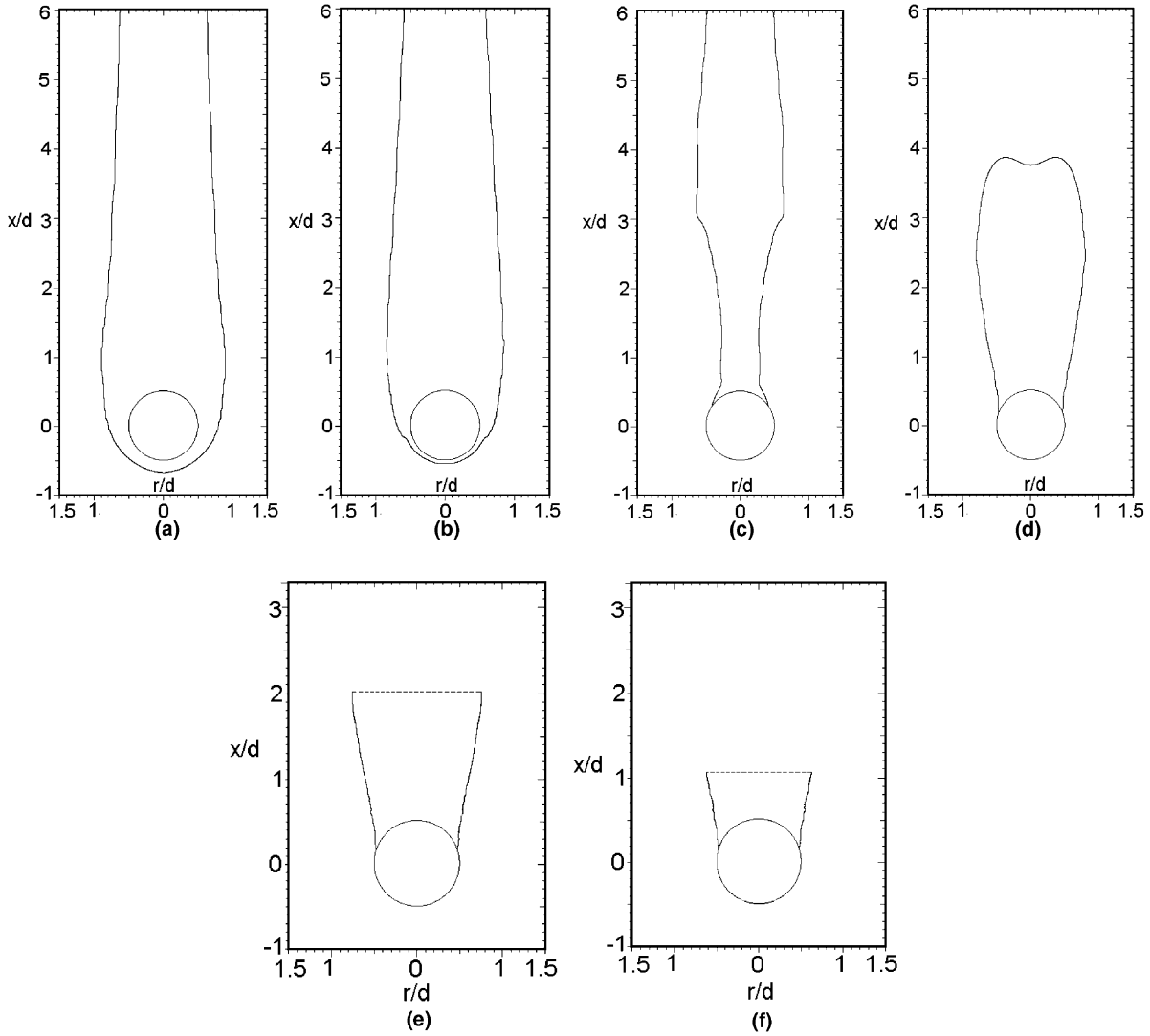

Fig. 12. Flame shapes for (a) $Re = 288$ (particle diameter = 10.8 mm, $u_\infty = 0.4$ m/s); (b) $Re = 864$ (particle diameter = 10.8 mm, $u_\infty = 1.2$ m/s); (c) $Re = 936$ (particle diameter = 10.8 mm, $u_\infty = 1.3$ m/s); (d) $Re = 2880$ (particle diameter = 10.8 mm, $u_\infty = 4$ m/s); (e) $Re = 4320$ (particle diameter = 10.8 mm, $u_\infty = 6$ m/s) and (f) $Re = 5760$ (particle diameter = 10.8 mm, $u_\infty = 8$ m/s).

increases, although the shape of the flame in the rear region is almost unaffected.

The equivalence ratio value ($\{F/O\}/\{[F/O]_{ST}\}$) at locations in the front portion of the droplet, for a case where an envelope flame exists, has been found to vary in between 0.818 and 0.958. This is in good agreement with the results reported in [19], where the authors have stated that the envelope flame is observed in the equivalence ratio range of 0.761 and 0.939.

When the free-stream velocity is increased beyond 1.25 m/s, the transition from envelope to wake flame occurs. The flame shape at a free-stream velocity of 1.3 m/s is shown in Fig. 12(c). There is no burning in the front portion of the sphere and the overall flame shape changes after this critical velocity. For a free-stream velocity of 4 m/s, the flame stabilizes in the wake region (Fig. 12(d)). For this wake flame case, the equivalence ratio in the front portion of the droplet has been evaluated to be in the range of 2.9–5.3 at different locations, indicating fuel rich zones in the front portion. As the free-stream velocity is increased to 6 m/s and 8 m/s, the flame height is reduced as can be seen in Fig. 12(e) and (f). In these cases, it was found that the region above the dotted line is highly mixed and a clear-cut delineation of fuel/oxidizer contour values to identify the flame boundary was not possible. Hence, as a measure of flame height, only the region where the boundary can be clearly identified has been indicated. With further increase in free-stream velocity, the flame eventually blows off. These trends (except for the flame shape in Fig. 12(c)) are in general agreement with the experimental flame shapes shown in Fig. 10. The flame shape at the instant of transition (corresponding to Fig. 12(c)) is extremely difficult to capture in the experiments because of the sudden changes associated with such instability.

5.2.3. Correlations for critical velocity and mass burning rate

The value of the free-stream velocity for which the flame transitions from envelope to a wake flame can be termed as the critical velocity. A correlation has been developed between the critical velocity and free-stream Reynolds number for given fuel and ambient conditions, using a parameter Γ defined as

$$\Gamma = 1.0 - \frac{v_s}{u_\infty}$$

In the above equation, v_s denotes the average evaporation velocity from the particle surface (obtained by dividing the average mass burning rate by the product of fuel density and particle surface area) and u_∞ is the free-stream velocity. The reason for the definition of Γ as above is explained as follows: although evaporation velocity increases with the free-stream velocity u_∞, the velocity ratio decreases, since evaporation velocity is proportional to square root of free-stream velocity ($v_s \propto u_\infty^{1/2}$). In order to have a monotonically increasing function of the free-stream velocity, Γ has been defined as above. Table 1 gives the critical values of free-stream velocity (u_∞) and Γ for different droplet diameters.

The average value of the parameter $\Gamma_{critical}$ is 0.906. It is reasonable to conclude from this table that the transition from envelope to wake flame would occur when $\Gamma_{critical} \approx 0.9$, at the ambient temperature of 300 K. In other words, when the evaporation velocity becomes 10% of the free-stream velocity (at $T_\infty = 300$ K), transition from envelope to wake flame occurs. It is also possible to estimate an equivalent flame speed (v_f) for this diffusion combustion problem, from the predicted reaction rates in the reaction zone. This flame speed is approximately of the order of the evaporation velocity v_s. For instance, calculating equivalent flame speed using the relation

$$v_f \approx \sqrt{\frac{\alpha}{\tau_{reaction}}}$$

gives $v_f \sim 0.05$ m/s and $\tau_{reaction} \sim 0.02$ s in a typical case, while $v_s \sim 0.1$ m/s. In this sense, the parameter Γ can be thought of as being related to the chemical and flow residence times. In terms of Reynolds number, an envelope flame would exist for $Re < Re_{crit}$ and a wake flame would prevail for $Re > Re_{crit}$.

The dimensionless mass burning rate (mass burning rate with flow ($\dot{m}$)/mass burning rate in the absence of flow ($\dot{m}_{ss}$) for spherico-symmetric combustion), has been

Table 1
Critical velocities and Γ for various cases

Particle diameter in mm	Critical velocity from experiments in m/s	Critical velocity from numerical data in m/s	$\Gamma_{critical}$ (based on numerical data)	Critical Reynolds number Re_{crit}
5	–	0.8	0.92	540
8	0.86	0.9	0.88	970
10.8	1.27	1.25	0.9	1800
12.2	1.3	1.3	0.905	2125
14	1.39	1.35	0.905	2530
16.4	1.44	1.4	0.915	3075
18.6	1.53	1.6	0.922	3985

correlated against the square-root of an effective Reynolds number defined as $Re_{\text{eff}} = Re_{\infty}(1 + \sqrt{Ri_{\infty}})$, where Ri_{∞} is the free-stream Richardson number. This effective Reynolds number takes buoyancy effects into account, which is quite important for low free-stream velocities and large fuel particle diameters. In the sub-critical range where the envelope flame exists, the correlation is of the form

$$\frac{\dot{m}}{\dot{m}_{\text{ss}}} = 0.09166\sqrt{Re_{\text{eff}}} - 0.28396$$

with a linear dependence on the square root of effective Reynolds number. In the super-critical range where the transition from the envelope to wake flame has occurred, the dimensionless mass burning rate turns out to be a quadratic expression of square root of effective Reynolds number, through the correlation

$$\frac{\dot{m}}{\dot{m}_{\text{ss}}} = 0.05392\sqrt{Re_{\text{eff}}} + 4.38936 \times 10^{-4} \times Re_{\text{eff}} - 0.08276$$

These correlation curves are shown in Figs. 13 and 14 respectively.

5.2.4. Contours of temperature and mass fractions of fuel and oxygen

Contours of temperature for the case of a 8 mm diameter sphere burning in a free-stream at 0.8 m/s and 4 m/s ($Re_{\infty} = 860$ and 4300 respectively) are shown in Fig. 15(a) and (b). Fig. 16(a) and (b) show the corresponding contours of fuel and oxygen mass fractions. These two cases clearly show an envelope flame and a wake flame. The reaction zone is identified by the occurrence of high temperature contours or low values of both fuel and oxidizer mass fractions.

In the case of a wake flame (Fig. 16(b)), although the fuel diffuses towards the front portion of the particle also, a combustible mixture of fuel and air is formed

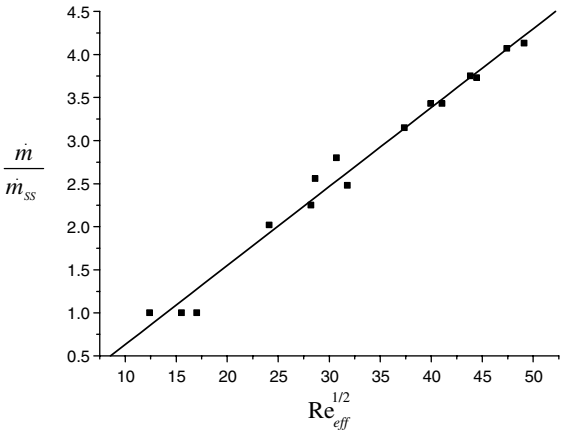

Fig. 13. Mass burning rate correlation for sub-critical Reynolds numbers.

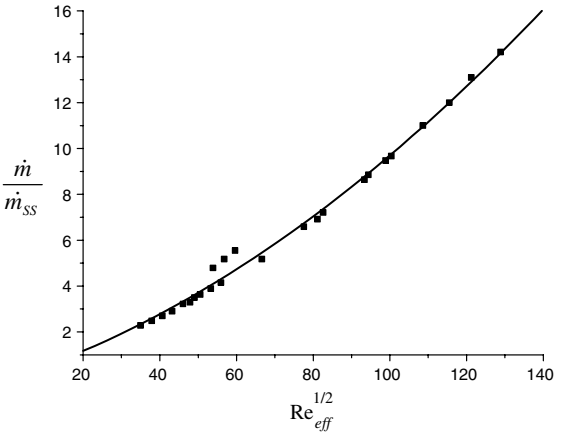

Fig. 14. Mass burning rate correlation for super-critical Reynolds numbers.

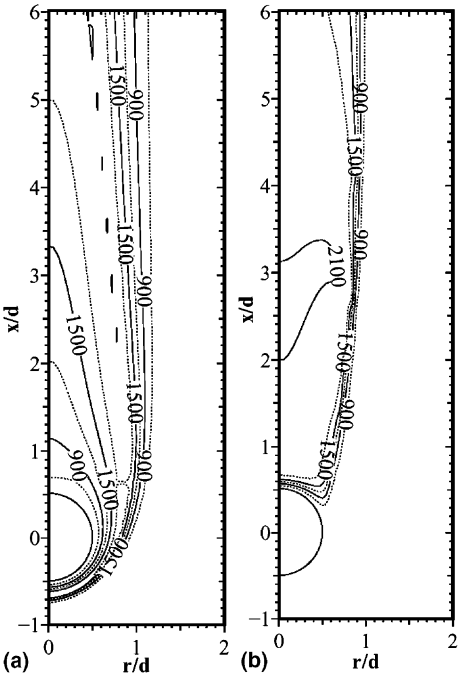

Fig. 15. Isotherms for a particle of diameter 8 mm: (a) $Re = 400$ ($u_{\infty} = 0.8$ m/s) and (b) $Re = 2000$ ($u_{\infty} = 4$ m/s).

only in the wake region due to high velocity air flow. Consequently, the highest temperature occurs in the wake region.

5.3. Effect of ambient temperature

For all the results presented so far, the ambient temperature has been kept at 300 K. In this section, the effect of different ambient temperatures on the burning

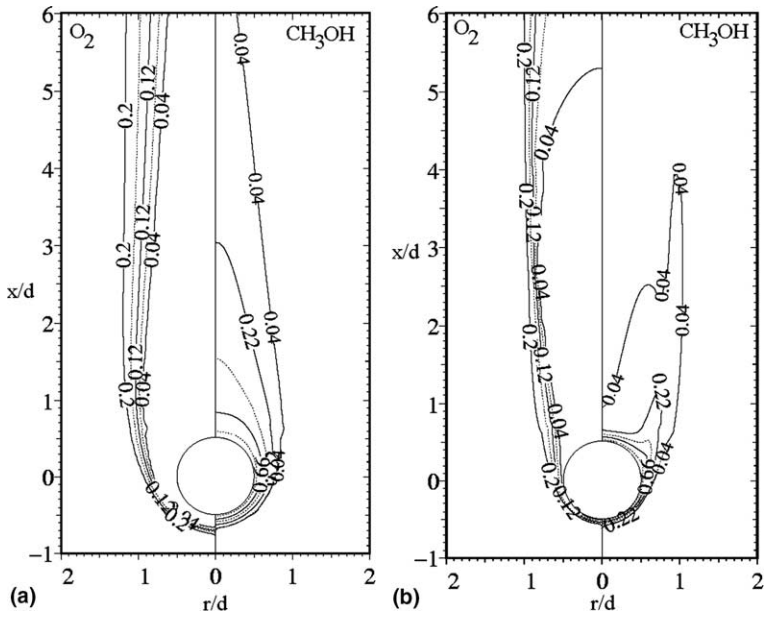

Fig. 16. Contours of mass fraction for a particle of diameter 8 mm: (a) $Re = 400$ ($u_\infty = 0.8$ m/s) and (b) $Re = 2000$ ($u_\infty = 4$ m/s).

of an 8 mm diameter particle is considered. The ambient temperature values considered are 300 K, 800 K and 1250 K. For each value of the ambient temperature, the free-stream velocity has been varied from 0.4 m/s to 12 m/s. Fig. 17(a) shows an envelope flame for all the above ambient temperature values. It is seen that the flame stand-off distance increases with ambient temperature. Fig. 17(b) shows an envelope flame for the ambient temperatures of 800 K and 1250 K but not for 300 K. This is due to the fact that the free-stream velocity of 1.2 m/s is higher than the critical velocity at 300 K. This shows that the transition from envelope to wake flame is delayed for higher ambient temperatures. For a free-stream velocity of 4 m/s and an ambient temperature of 300 K (Fig. 17(c)), it is observed that the flame has completely stabilized in the wake region of the sphere. But for higher ambient temperatures, transition is yet to occur; however, the flame standoff distance has reduced considerably, especially in the front portion of the fuel particle.

Flame shapes corresponding to a free-stream velocity of 8 m/s are shown in Fig. 17(d). For the ambient temperature of 300 K, the wake flame height has decreased drastically and for 800 K case also, transition from envelope to wake flame has occurred. However, for the ambient temperature of 1250 K, transition is yet to occur even though the flame stand-off distance has decreased further. Fig. 17(e) and (f) show the flame shapes at the free-stream velocities of 10 m/s and 12 m/s respectively, for the ambient temperatures of 800 K and 1250 K. For these free-stream velocities, the flame has blown off for the ambient temperature of 300 K and so the corresponding curves are not provided in the figures. It is evident that even for a free-stream velocity as high as 12 m/s, there is still an envelope flame at the ambient temperature of 1250 K. This is due to the fact that the enhanced reaction rate at the higher ambient temperature enables rapid burning of the fuel vapor. The dimensionless mass burning rate at different free-stream velocities is almost independent of the ambient temperature [10]. Thus the mass burning rate correlations developed in the previous section for the ambient temperature of 300 K can be used for other ambient temperature values also without much error.

The variation of the critical value of Γ (for transition from envelope to wake flame) with ambient temperature is shown in Fig. 18. It is seen that the critical value of Γ increases with ambient temperature and asymptotically reaches unity. The critical free-stream Re for 8 mm particle diameter at 300 K is 970 and at 800 K it is 7550. But for the case of 1250 K ambient temperature, the transition from envelope flame does not occur even at a free-stream velocity of 12 m/s ($Re = 13\,000$). Using the current laminar model, further parametric study using higher free-stream velocity values is not possible, since wake becomes turbulent.

6. Conclusions

Unsteady burning of a single particle in a mixed convective environment has been simulated numerically

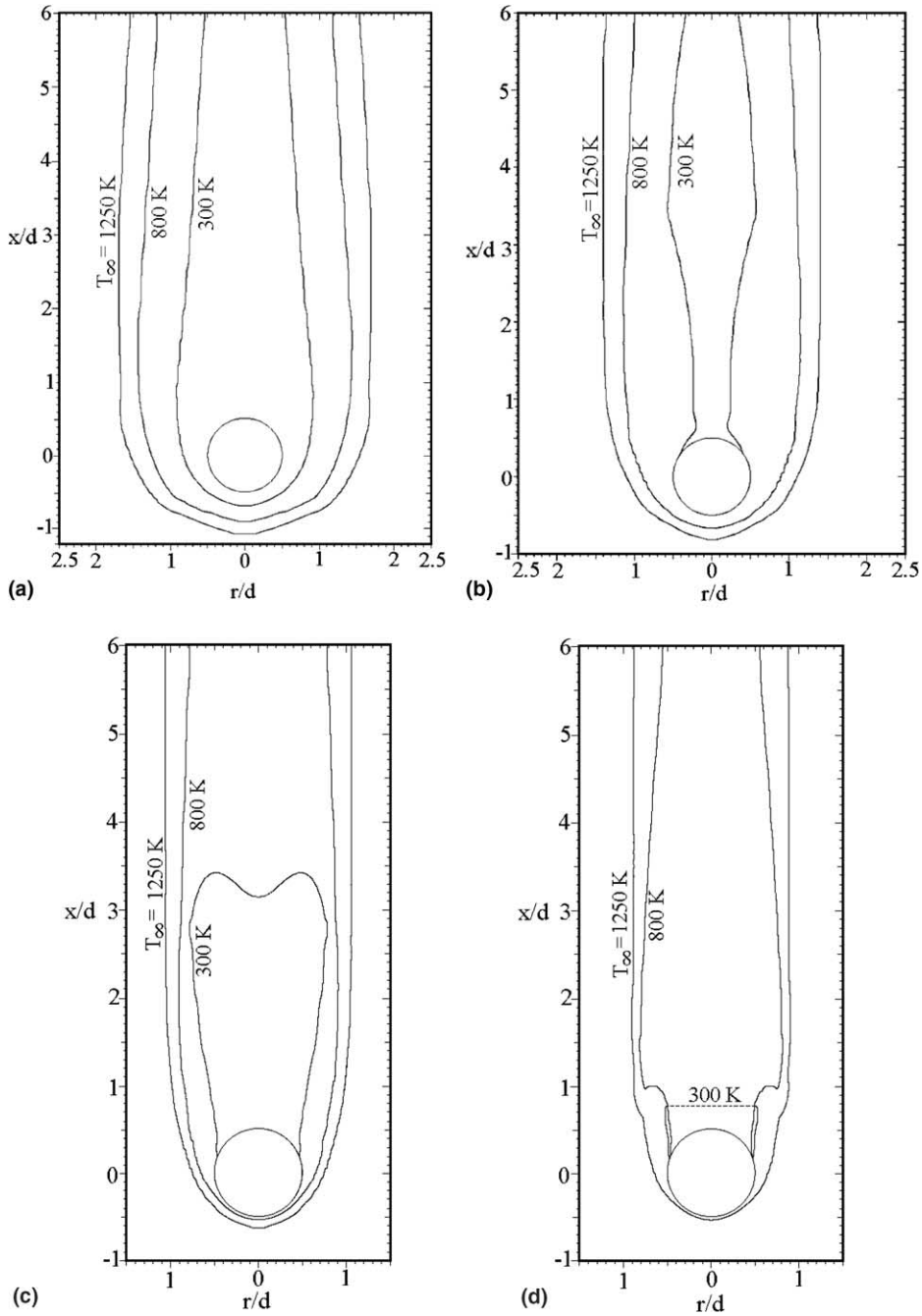

Fig. 17. Flame shape variation with free-stream temperature for a particle of 8 mm diameter: (a) $Re = 200$ ($u_\infty = 0.4$ m/s), (b) $Re = 600$ ($u_\infty = 1.2$ m/s), (c) $Re = 2000$ ($u_\infty = 4$ m/s), (d) $Re = 4000$ ($u_\infty = 8$ m/s), (e) $Re = 5000$ ($u_\infty = 10$ m/s) and (f) $Re = 6000$ ($u_\infty = 12$ m/s).

using both infinite and finite rate chemistry models with variable mixture properties. The problem has also been studied experimentally using the porous sphere technique. The numerical predictions show good agreement with experimental data obtained in the present study as well as with those reported in literature. It is seen that both infinite rate and finite rate chemistry models predict the flame shapes and mass burning rates accurately at low free-stream velocities, when an envelope flame exists. In fact the predictions show a

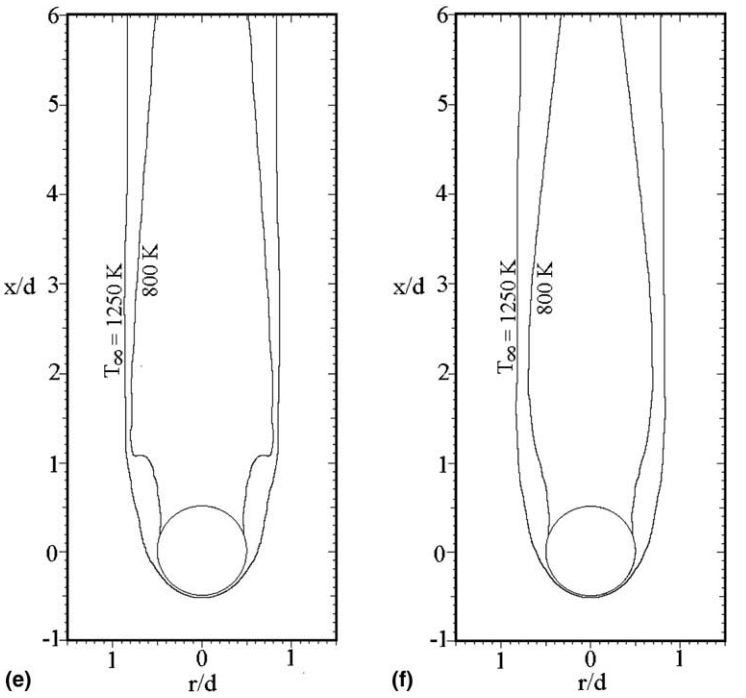

Fig. 17 (*continued*)

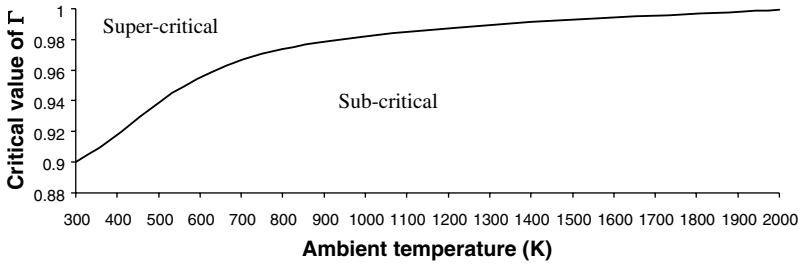

Fig. 18. Variation of critical value of Γ with ambient temperature.

laterally flattened flame shape when the free-stream air flow and the buoyancy driven convective flow around the particle are in opposing configuration. As the free-stream velocity is increased, the flame stand off distance in the front portion of the droplet decreases; at a critical value of the free-stream velocity, transition occurs from envelope flame to wake flame. The mass burning rate generally increases with free-stream velocity, but suffers a sudden decrease at transition from envelope to wake flame. For free-stream velocity values above the critical value (super-critical range), a stabilized flame occurs in the wake region. With further increase in the free-stream velocity, the height of the wake flame reduces and eventually the flame is blown off. This sequence of phenomena is observed experimentally and they are also correctly predicted by the finite rate chemistry model with variable properties. The infinite rate chemistry model, however, does not predict transition, occurrence of wake flame and flame blow off. This implies that the transition phenomena are caused by the competition between convection (or the flow residence) and chemical kinetic processes. Correlations have been developed in non-dimensional form on the basis of the present study for the critical velocity and the mass burning rate at sub-critical as well as super-critical ranges of free-stream velocity. The critical free-stream velocity for the transition to wake flame increases with ambient temperature. The dimensionless mass burning rate, however, is relatively insensitive to changes in the ambient temperature.

References

[1] H.S. Caram, N.R. Amundson, Diffusion and reaction in a stagnant boundary layer about a carbon particle, Ind. Eng. Chem. Fundam. 16 (2) (1977) 171–181.

[2] E. Mon, N.R. Amundson, Diffusion and reaction in a stagnant boundary layer about a carbon particle. 2. An extension, Ind. Eng. Chem. Fundam. 17 (4) (1978) 313–321.

[3] M.K. King, Ignition and combustion of Boron particles and clouds, J. Spacecraft 19 (4) (1982) 294–306.

[4] H. Isoda, S. Kumagai, Combustion of fuel droplets in a falling chamber, in: Sixth Symposium (International) on Combustion, Combustion Institute, 1955, pp. 726–731.

[5] A. Chervinsky, Transient burning of spherical symmetric fuel droplets, Israel J. Technol. 7 (1969) 35–42.

[6] S. Kumagai, T. Sakai, S. Okajima, Combustion of free fuel droplets in a freely falling chamber, in: Thirteenth Symposium (International) on Combustion, Combustion Institute, 1971, pp. 779–785.

[7] T.A. Brzustowski, R. Natarajan, Combustion of aniline droplets at high pressures, Canad. J. Chem. Eng. 44 (1966) 194–201.

[8] S.R. Gollahalli, T.A. Brzustowski, Experimental studies on the flame structure in the wake of a burning droplet, in: Fourteenth Symposium (International) on Combustion, The Combustion Institute, 1973, pp. 1333–1344.

[9] H.A. Dwyer, B.R. Sanders, A detailed study of burning fuel droplets, in: Twenty-First Symposium (International) on Combustion, Combustion Institute, 1986, pp. 633–639.

[10] S.Y. Cho, R.A. Yetter, F.L. Dryer, A computer model for one-dimensional mass and energy transport in and around chemically reacting particles, including complex gas-phase chemistry, multi-component molecular diffusion, surface evaporation and heterogeneous reaction, J. Comput. Phys. 102 (1992) 160–168.

[11] P. Balakrishnan, T. Sundararajan, R. Natarajan, Interference effects during burning of tandem porous spheres in mixed convective environment, AIAA J. 38 (2000) 1889–1898.

[12] P. Balakrishnan, T. Sundararajan, R. Natarajan, Combustion of a fuel droplet in a mixed convective environment, Combust. Sci. Technol. 163 (2001) 77–106.

[13] T.R. Blake, Low Reynolds number combustion of a spherical carbon particle, Combust. Flame 129 (2002) 87–111.

[14] C.H. Chiang, M.S. Raju, W.A. Sirignano, Numerical analysis of convecting, vaporizing fuel droplet with variable properties, Int. J. Heat Mass Transfer 35 (5) (1992) 1307–1324.

[15] J. Sato, M. Tsue, M. Niwa, M. Kono, Effects of natural convection on high pressure droplet combustion, Combust. Flame 82 (2) (1990) 142–150.

[16] H.T. Zhang, Numerical research on a vaporizing fuel droplet in a forced convective environment, Int. J. Multi-Phase Flow 30 (2004) 181–198.

[17] M. Renksizbulut, M.C. Yuen, Experimental study of droplet evaporation in a high temperature air stream, J. Heat Transfer Trans. ASME 105 (1983) 384–388.

[18] W.A. Sirignano, Fuel droplet vaporization and spray combustion theory, Prog. Energy Combust. Sci. 9 (1983) 291–322.

[19] G.A. Szekely Jr., G.M. Faeth, Effects of envelope flames on drop gasification rates in turbulent diffusion flames, Combust. Flame 49 (1983) 255–259.

[20] V. Raghavan, Modeling of unsteady effects during spray droplet burning, Ph.D. thesis, Indian Institute of Technology Madras, Chennai, India, 2004.

[21] R.C. Reid, J.M. Prausnitz, T.K. Sherwood, The Properties of Gases and Liquids, third ed. McGraw-Hill Book Company.

[22] R.S. Turns, An Introduction to Combustion: Concepts and Applications, McGraw-Hill Book Company, 2000.